Fermi National Accelerator Laboratory

FERMILAB-Pub-85/121-E
7620.740

HADRON SHOWERS AND MUON TRAJECTORIES IN THICK ABSORBER FROM 25 GeV/c to 150 GeV/c*

D. Green, H. Fenker, P. Martin, M. Takasaki, and R. Yamada
Fermi National Accelerator Laboratory, Batavia, Illinois 60510

and

S. Kunori and P. Rapp
University of Maryland, College Park, Maryland 20742

and

D. Owen
Michigan State University, East Lansing, Michigan 48824

and

P. Grannis and D. Hedin
State University of New York at Stony Brook, Stony Brook, New York 11794

September 1985

*Submitted to Nuclear Instruments and Methods A

HADRON SHOWERS AND MUON TRAJECTORIES IN THICK ABSORBER FROM 25 GeV/c TO 150 GeV/c

D.GREEN, H.FENKER, P.MARTIN, M.TAKASAKI,
R.YAMADA
Fermi National Accelerator Laboratory,
Batavia, Illinois 60510, U.S.A.

S.KUNORI, P.RAPP
University of Maryland,
College Park, Maryland 20742, U.S.A.

D.OWEN
Michigan State University,
East Lansing, Michigan 48824, U.S.A.

P.GRANNIS and D.HEDIN
State University of New York at Stony Brook,
Stony Brook, New York 11794, U.S.A.

Hadron shower punchthrough and muon momentum measurements were conducted at 25, 50, 100 and 150 GeV/c, using tracking before, between and after a 7.3 interaction length (λ_0) lead block and 7.3 λ_0 of magnetized iron. The multiplicity and spatial distributions of both hadrons and muons were obtained. Muons were used to study the multiple scattering, the effect of δ rays and associated phenomena, and the momentum resolution. Hadrons were used to study the muon/hadron rejection factor. The measured punchthrough probabilities after 7.3 and 14.6 λ_0 were consistent with other data. Cuts are described which define the final rejection factor against hadrons.

1. Introduction

The observation of muons from high energy interactions has played an important role in discoveries and studies of new particles and new phenomena in high energy physics. The decays of $J/\psi \rightarrow \mu^+\mu^-$ and $\Upsilon \rightarrow \mu^+\mu^-$ are examples of new particle production. The more recent discovery of the vector bosons, with decays $W^{\pm} \rightarrow \mu^{\pm}\nu$ and $Z^0 \rightarrow \mu^+\mu^-$, in the CERN $\bar{p}p$ collider experiments again proved the importance of the detection of muons. Muon decay products are expected to figure prominently in new phenomena, given current theoretical speculation [1].

The detection of muons consists of two parts, the identification of muons and the measurement of their charge and momentum. The standard identification technique is to have thick material absorb all other particles and then measure the muons exiting from the absorber. The hadrons, electrons and photons are absorbed in the cascade shower process in the thick absorber. The probability of leakage of the shower particles increases with the energy of the parent particles. To cleanly identify muons one must keep the leakage probability small and also have the ability to reject any leaking shower particles. The momentum measurement of muons is done by a combination of a magnetic field and tracking detectors. Delta rays, bremsstrahlung

and e^+e^- pair creation associated with muons obscure the muon track in the tracking detectors.

The proposed DO detector [2] for the Fermilab $\bar{p}p$ collider experiment will detect muons by using magnetized iron toroids following the uranium-liquid argon calorimetry. The large amount of material (7 λ_0 of calorimetry and 6 λ_0 of iron at θ=90°) will absorb most hadron showers. Muon tracking will be done using large array of proportional drift tubes before and after the iron toroids and the central tracking system.

There are several experimental measurement of hadron shower development and hadron punchthrough probabilities in the energy region of 25 to 150 GeV. Data from experiments completed prior to 1979 on hadron shower development are compiled elsewhere [3]. Later data include an extensive study of the hadron punchthrough probability carried out at CERN [4]. The WA1 experiment at CERN has reported data taken from 15 to 140 GeV with sandwiches of thin steel plates and scintillators to study the detailed longitudinal and lateral development of hadron showers, and the energy resolution for a hadron calorimeter [5]. Most recently an experiment to study hadron punchthrough in iron at depths up to 250 cm was carried out at Fermilab from 12 to 200 GeV/c [6].

The tests reported here were conducted during the spring of 1984 in the NW test beam at Fermilab using a detector setup which closely simulated the proposed DO detector. The purpose of this test was to obtain the following data, which were essential in finalizing the design of the DO detector and which could not be obtained from published data;

1) Hadron punchthrough probability after a thick absorber.

2) Measurement of mean associated multiplicity and spatial distribution of tracks in remnant hadron showers.

2. Experimental layout

The layout of the apparatus is shown in fig. 1. The incident beam momentum is measured by the last bending magnet (BM) in the beam line and four proportional wire chambers (PWC), W1 to W4. Then the incident particle is tagged by 3 scintillators S0, S1 and S2 and a PWC, W5. A halo counter (SH) is used in veto. The last three sets, W3, W4 and W5, determine the incident particle direction and position. The beam track tagging is followed by 1413 g/cm^2 (124.5 cm) of lead bricks (CC) which roughly equals the mean density in the DO uranium liquid argon calorimeter. This corresponds to 7.3 λ_0, 1.6 GeV minimum ionization energy loss and 222 radiation lengths (X_0). Particles exiting CC

are detected by the scintillation counter S3 and two chambers of proportional drift tubes (PDT), D1 and D2, together comprising station A.

Following station A, there is magnetized iron (CF) (960 g/cm^2, 122 cm, 7.3 λ_0, 1.4 GeV minimum ionization loss, 69 X_0). Particles behind CF are detected by a scintillation counter, S4, and three PDT chambers, D3, D4 and D5 which comprise station B.

Approximately 10 meters downstream of the magnet, there is a beam dump consisting of 2.7 m of iron and 0.7 m of concrete. A set of muon tag counters (S5 and S6) is located behind the dump, and is used for tagging muons. The status of MU=S5·S6 is logged with the data. S5 is at 15 cm behind the dump and S6 at 1250 cm further behind S5. The sizes of detectors are given in Table 1.

Each PWC consists of 2 layers in each of the horizontal (X) and vertical (Y) coordinate. Each layer has 64 wires at 1 mm spacing with adjacent layers assembled with an offset of 0.5 mm. These chambers are intended to be a simulation of DO central tracking system.

Each PDT chamber also consists of 2 layers offset by a half cell width in each of the horizontal and vertical views. The cells are made of 2.5 cm x 2.5 cm drift tubes [7]. These tubes are operated with argon/ethane (1:1 mixture) in a saturated drift mode with approximately 250 nsec maximum drift time. This system is intended to simultate the geometry of the D0 muon detectors but to have added granularity and redundancy. Thus, one can study the effects of these variables on muon detection efficiency and hadron rejection power.

3. Experimental runs and data analysis

The incident beam was mainly negative pions with a few percent muons. The momentum was nominally 25, 50, 100, and 150 GeV/c. The momentum bite was 1.4% (full width at half maximum, FWHM), at 150GeV/c.

To check the alignment of the whole system, straight through runs were made periodically with CC and CF out of the beam line. The accuracy of the alignment is about 0.5 mm (FWHM).

Two triggering procedures were used. They were defined as follows:

Beam trigger = S1·S2 = BEAM

Standard trigger = BEAM·S3·S4 = ST

Due to limited beam time, the system was mostly triggered using ST which enhances the number of punchthrough events by requiring a particle after CC and CF. The purpose of the Beam trigger was to look for biases in ST. Using the Beam trigger data we measured the inefficiencies of S3 and S4, and corrected for this inefficiency. At all 4 momenta we took triggers (using ST) corresponding to 10^6 incident beam tracks. At each momentum data were taken with the magnet, CF, on and off alternately. At 150 GeV/c and 50 GeV/c we took 10^4 and 10^5 unbiased beam triggers, respectively.

The incident particle trajectory is determined by PWC W3, W4 and W5. To ensure single beam tracks we only use events with a single cluster of hits, i.e. one hit or two hits on adjacent wires, in W5.

The PDT signals are processed through several steps. In each plane the signals from the two offset layers are searched for pairs giving positions consistent within 5 mm. The consistency check is that the sum of the two drift times equals the wire spacing. The paired signals define a plane hit. Layer hits which are inconsistent are ignored.

The multiplicity of a plane is the number of plane hits. The station multiplicities, n_A (n_B), are defined to be the largest plane multiplicity in the four (six) planes in station A (B). The X or Y position of each plane hit is calculated with respect to the extrapolated position of the incident particle trajectory.

The geometrical acceptance of the muon tag counters, S5 and S6, was calculated using a simple Monte Carlo program implementing multiple Coulomb scattering in the absorbers. It was also calculated from the data. The results were consistent; the acceptance is 0.35, 0.78, 0.94 and 0.97 for muons at 25, 50, 100 and 150 GeV/c respectively with the magnet off. This finite acceptance means that an auxiliary method to separate muons and hadrons is needed.

We define two sets of muon samples. The first set (SET1) is defined to be triggers with the MU flag set. An additional set (SET2) is defined in the $\overline{\text{MU}}$ data at 50 and 25 GeV/c in order to avoid the inefficiency and bias of the muon tag counters at low momenta. This set is defined to be triggers with multiplicities equal to 1 in both station A and B. The hadron contamination in SET2 is negligible, with less than 1% hadrons in SET1 or SET2.

We have defined a figure of merit to parametrize the lateral distribution: $R^B_{max} = [X^2_{Bmax}+Y^2_{Bmax}]$ where X_{Bmax} and Y_{Bmax} are the largest X and Y values from the three X and three Y planes in station B. R^B_{max} is the effective radius of the shower in station B.

In order to separate hadrons from muons in the $\overline{MU}$ data set, we cut on R^B_{max}. The cut value is 525(cm)/P(GeV/c) and scales with the multiple scattering of muons. About 90% of the muons survive this cut at all momenta. In contrast, only 1, 3 and 15 % of the hadron events survive this cut at 150, 100 and 50 GeV/c respectively. Details of the R^B_{max} distribution are described in the Appendix.

4. Experimental results

4.1 Muon Distributions

The muon (SET1) multiplicity distributions, n_A and n_B, at station A and B are shown in fig. 2. In both stations approximately 10% of all muons have a multiplicity $= 2$ at all energies. Fig. 3 shows the fraction of events with $n \geq 2$. These events are mostly due to accompanying δ rays. As expected, the fraction is only weakly momentum dependent. Note that the critical energy for muons in iron is 300 GeV, where energy loss due to radiation becomes larger than that

due to ionization[8]. About 1% of the muon events at 150 GeV/c have an accompanying shower. This rate is roughly that expected for muon bremsstrahlung and pair production. In this environment tracking seems hopeless.

Figure 4 shows the distributions of X-positions at the D2 and D4 planes for muons (SET1 + SET2) at all 4 momenta. The dashed histograms are for muons unaccompanied by any other track. The dashed curves are Gaussian fits to these distributions. Evidently, the Gaussian fit is acceptable even after a traversal of 290 X_0.

In fig. 5 we show the X-distribution of muons plus accompanying particles for muon events with multiplicity greater than one at 150 GeV/c. Also shown is a proposed D0 PDT cell size. Clearly the δ rays are tightly clustered around the muon, necessitating multi-hit electronics in order to preserve full detection efficiency.

We also fit Gaussians to the angular distributions and the projected position distributions at the downstream ends of CC and CF. Figure 6 shows the widths in the Gaussian fit. The solid and dashed lines are calculated using standard shower theory [8]. Although this theory is presumed to be accurate only for relatively thin material, it agrees with our data to within about 20%.

4.2 Muon Momentum Resolution

We measured the incident muon momentum using PWC's W1 through W4. The momentum was then remeasured using the PDT chambers before and after the magnetized iron. The resolution is limited at the low momentum end by multiple scattering in the iron, and for high momentum particles by position resolution and the two lever arms.

The effects contributing to muon momentum resolution are multiple Coulomb scattering and PDT measurement errors. Therefore the resolution can be written as follows:

$$\frac{\Delta\ 1/P}{1/P} = \left[\ \alpha^2 + (\beta P)^2\ \right]^{1/2}$$

where the first and second terms correspond to multiple Coulomb scattering and measurement error, respectively. Additional effects on resolution are due to the incident beam momentum bite and to low momentum muons from pion decay in flight after passing the last bending magnet in the beam channel.

The momentum resolution is shown in fig. 7 as a function of measured momentum. The closed and open points in fig. 7 indicate the momentum resolution before and after the corrections for decay muons. The resolution coefficients α and β are α=0.181 and β=2.40x10^{-3} per (GeV/c). The two contributions are shown separately in fig. 7. The coefficient of the measurement term corresponds to a PDT alignment accuracy of 450 μm. Note that PWC W5 was not used in this analysis. In the DO experiment a central tracker will be used at high momentum to reduce the β coefficient such as to be small with respect to α out to P_T = 200 GeV/c.

4.3 Hadron Distributions

The multiplicity distributions of hadron events ($\overline{MU}$ events with R^B_{max} outside the cut) are shown in fig. 8 for the 50, 100 and 150 GeV/c data sets. The contamination from muons has been subtracted from these distributions by estimating the fraction of muons falling outside the cut and using the distributions for the muon events shown in fig. 2. Since the cut removes only 15%, 3% and 1% of the real hadron events for 50, 100 and 150 GeV/c respectively, no hadronic corrections are made.

The mean multiplicities, $\bar{n}$, show a slow increase with momentum. These multiplicities are underestimated because of the limited size of the PDT's, (See Table 1) especially D1 and D2 in station A. Figure 9 shows the correlation between the multiplicities in A and B stations. No evidence for any correlation was seen, as expected in a randomly evolving shower.

Figure 10 shows the distributions in X-position in stations A and B. The solid histograms are for the 150 GeV/c hadron event sample with the ST trigger and the dashed for the Beam trigger data. The muon contamination has been subtracted. The distribution for the ST trigger data (solid) is narrower than that for the Beam trigger data (dashed). This is an indication of trigger bias since the ST trigger events, which are required to reach the end of the absorber, typically interact deeper in the absorber. Thus the shower has not yet fully developed in the transverse direction.

Specifically, the events in the shaded area are those with the multiplicity $n_A = 1$, and their X-distribution is within the multiple scattering limit observed in fig. 4 for muons. These events are indeed hadrons and are due to non-interacting hadrons in the lead absorber which is an extreme case of trigger bias towards late developing

showers. The event rate for this peak agrees well with the calculated rate of non-interacting hadrons using the nominal attenuation length [8] in lead.

After subtracting these non-interacting events, one has a distribution which can be approximated by a Lorentz line shape. Fits to the data are shown in fig. 10 as solid lines. The fitted values of Γ, (FWHM), are shown in fig. 11. The increase in size of the shower in station B, is consistent with approximately 100 mrad mean angle of the hadronic shower particles. The ratio of Γ's in station A and B is 1.8. A scaling in $\rho L(g/cm^2)$ units for the lateral shower size has been reported[3], and our ratio roughly agrees with that scaling. Note that there is only a weak momentum dependence of the shower sizes.

4.4 Hadron Punchthrough Probability

The hadron punchthrough probability, P_h, is defined to be the ratio of the number of hadron events in the ST sample to the total number of incident hadrons. In this section we calculate P_h at two depths of absorber, at station A (7.3 λ_o, 1413 g/cm^2) and B (14.6 λ_o, 2373 g/cm^2).

Due to the lack of unbiased Beam trigger data at all momenta, P_h at station A (B) is obtained using the scaler count for S1·S2 (=BEAM) and that for BEAM·S3 (BEAM·S3·S4). The scaler for BEAM counts the number of beam particles and that for BEAM·S3 (BEAM·S3·S4) counts the number of events reaching station A (B). The fraction of muons in the beam is estimated to be 8.5, 6.7 and 3.4 % for 50, 100 and 150 GeV/c respectively(Appendix). After subtracting the muons, P_h as a function of momenta is shown in fig. 12. A 20 % systematic error has been assigned to the values of P_h.

For comparison, the measurments from other experiments [5,6,9] are also shown in fig. 12. The P_h from all other experiments are for iron absorber. Note that P_h from Ref. 6 is calculated from the distributions of the number of wire hits. The P_h for lead from this experiment is smaller than that for the same number of λ_0 of iron from other experiments. In fact, 1 λ_0 only defines the mean depth for a shower to begin, while details of late shower development obviously also depend on X_0 and ρL (g/cm^2) [4,10]. Note that the failure of λ_0 scaling in a Pb calorimeter has previously been noted by the UA1 group[4].

Moreover, there is a factor of 2 discrepancy between the E636 and WA1 data sets in iron at the same depth. Note also that S3, which determines P_h at station A, is only 25.4

x 25.4 cm^2. Some punchthrough events fall outside of S3 (See fig. 10). As seen in fig. 12 our data in station A falls between λ_0 scaling and ρL scaling in comparison to the data from other experiments. In station B our data is consistent with ρL scaling to the CCFR data.

The 100:1 punchthrough rejection is not sufficient for the muon system of the DØ experiment. Additional rejection power using the multiplicity and the hit position(s) at the two stations, A and B, is required. Note that muons have R values within a multiple scattering limit (see fig. 4), while hadrons have R values on the scale of ρL (see fig. 10). The data in fig. 12 called Coulomb cut are defined as follows. Events with $\overline{MU}$ are required to have multiplicity at station B, $n_B=1$, and R^B_{max} within the cut discussed in Section 3. A further cut requires $R^A_{min} < R^A_{cut}$, where $R^A_{min} = [X^2_{Amin}+Y^2_{Amin}]^{1/2}$. X_{Amin} and Y_{Amin} are the smallest X and Y values from the two X and two Y planes in station A. R^A_{cut} is given as [100/P(GeV/c)] cm. The cut on R^A_{min} defines a cone at station A in which 90 % of all muons are contained. The cuts at station B reject about 10 % of all muon events due mostly to δ rays associated with the muons. The Coulomb cut rejects about 20% of all muons, while hadron punchthrough events are rejected by factors of, 16, 174 and 575 for 50, 100 and 150 GeV/c respectively. As seen in fig. 12, the Coulomb cut leads to $> 10^4$ hadron

rejection for > 50 GeV/c hadrons. The rejection factor improves with momentum, extrapolating to > 10^5 for > 200 GeV/c hadrons.

5. Conclusion

We measured muon trajectories and hadron punchthrough from 25 to 150 GeV/c using tracking detectors before and after a lead block (7.3 λ_0, 1413 g/cm^2) and after magnetized iron (7.3 λ_0, 960 g/cm^2). The multiplicities and spatial distributions were measured for both muons and hadrons. The momentum resolution for muons was obtained.

About 10% of the muon events are accompanied by particles due to δ rays, bremsstrahlung or e^+e^- pairs. They are mostly distributed in a 5 cm radius around the muon. This suggests that fine segmentation or multihit capability is needed in muon tracking detector for efficient operation.

The hadron punchthrough probability after 14.6 λ_0 (2373 g/cm^2) is (0.14 to 1.1)x10^{-2} from 50 to 150 GeV/c. This probability is consistent with other data measured in iron. An approximate scaling in ρL (g/cm^2) units is suggested in comparison with other data. Using the exit positions and angles of the punchthrough tracks (the Coulomb cut) yields additional rejection factors. The rejection

power of the Coulomb cut increases with energy. The hadron punchthrough probability after the Coulomb cut is (7.1 to 2.1)x10^{-5} for momenta of 50 to 150 GeV/c.

We wish to thank Dr. K. Yasuoka for the helpful discussions during this work.

Appendix. R^{B}_{max} distribution.

The last MU counter is located about 30 m downstream from the front end of the lead block, and it subtends about ± 10 mrad with respect to the beam axis. Due to multiple scattering, its acceptance is large for higher energy muons but small for lower energy muons. Therefore some real muon events do not have a MU tag, especially in the lower momentum data, and auxiliary methods of discriminating hadrons and muons must be used for the $\overline{MU}$ data.

The muon trajectory has a small value of $R(=[X^2+Y^2]^{1/2})$ whose value is set by the multiple Coloumb scattering, and hence scales as 1/P. Hits due to shower particles from a hadron are spread out in R in a roughly momentum independent spectrum whose scale is set by ρL (g/cm^2)[3]. Thus, in order to maximize the separation of muons and hadrons in the R distribution we introduce a quantity R^{B}_{max}, which is defined in Sec. 3.

Shown in fig. 13 are the R^{B}_{max} distributions for MU events. The data at 25 GeV/c is excluded because of the poor geometric efficiency of the MU counter (about 35%) at that energy. Peaks at small R^{B}_{max} become wider as 1/P which is consistent with the multiple scattering of muons. The long tail is due to accompanying δ rays, bremsstrahlung,

e^+e^- pair production, or accidentals.

The R^B_{max} distributions for $\overline{MU}$ events are shown in fig. 14. Peaks are again seen at small R^B_{max}. In addition to a peak at the small R^B_{max} in the 150 GeV/c data (fig. 14a), there is an excess at large R^B_{max}. Clearly some muon leakage exists.

In order to see the R^B_{max} distributions for purely hadron events we apply a further cut on $R^A_{min} = [X^2_{Amin}+Y^2_{Amin}]^{1/2}$, which is defined in Sec. 4.4. The R^A_{min} distributions for MU events show that less than 4% of all muons are contained in a region defined by $R^A_{min} > R^A_{cut}$, where R^A_{cut} is chosen to be [150/P(GeV/c)] cm. This cut value is 1.5 times larger than that used in Sec. 4.4 in order to more cleanly exclude muons. Shown in fig. 15 are the R^B_{max} distributions for the $\overline{MU}$ events with $R^A_{min} > R^A_{cut}$. The curves in fig. 15 are a result of a polynomial fit to the 150 GeV/c data (fig. 15a) and are normalized to the distributions for the other data. The R^B_{max} distributions with the R^A_{min} cuts have only a weak momentum dependence.

The same curve is also shown in fig. 14. Considering the peak in the MU data (fig. 13) and the R^B_{max} distributions for hadrons (fig. 15), we conclude that the R^B_{max} distribution for $\overline{MU}$ events (fig. 14) consists of two

components, one due to muons which fail to set the MU bit and a second due to hadrons represented by the shape seen in fig. 15a. A schematic graph of the two components is shown in fig. 16.

In order to estimate the number of muons and hadrons in the $\overline{MU}$ data we solve the following equations.

$$N_{\mu 1} + N_{h1} = N_{obs1} \quad (\text{for } R^B_{max} < R^B_{cut}) \qquad (A1)$$

$$N_{\mu 2} + N_{h2} = N_{obs2} \quad (\text{for } R^B_{max} > R^B_{cut}) \qquad (A2)$$

where R^B_{cut} are chosen to be [525/P(GeV/c)] cm in order to scale with multiple Coulomb scattering. $N_{\mu 1}$, N_{h1} and N_{obs1} are the number of muons, hadrons and observed events in the smaller R^B_{max} region. $N_{\mu 2}$, N_{h2} and N_{obs2} are those in the larger R^B_{max} region.

We make two assumptions to solve the equations.

1. The R^B_{max} distributions for hadrons are the same for all energies and are given by fig. 15a. This assumption gives the ratio N_{h1}/N_{h2}.

2. The ratio $N_{\mu 1}/N_{\mu 2}$ is equal to that in the MU events as seen in fig. 13.

The results are given in Table 2 with the number of MU events.

From Table 2 we may calculate the efficiencies of the MU counters and the fraction of muons in the beam. The fraction of muons in the beam is 3.4, 6.7 and 8.5%, while the geometric efficiency of the MU tag counters is 97, 94 and 78% for 150, 100 and 50 GeV/c, respectively.

	x(cm)	y(cm)
S1, S2	7.8	7.8
S3	25.4	25.4
S4	63.5	35.6
S5	76.0	82.0
S6	74.0	61.0
W1 ~ W5	6.4	6.4
D1, D2	17.8	17.8
D3	35.6	17.8
D4, D5	73.7	35.6

Table 1. Sizes of scintilators, PWC chambers and PDT chambers.

P (GeV/c)	Beam $x10^5$	$\overline{MU}$				MU
		N_{h1}	N_{h2}	$N_{\mu 1}$	$N_{\mu 2}$	
150	2.40	38.8±7.6	2579.8±55.4	195.3±16.8	39.2±3.6	7973
100	1.84	42.3±5.7	1240.0±38.1	630.7±27.0	67.0±3.5	11630
50	0.92	18.0±3.3	102.1±17.1	1621.0±43.2	137.0±7.5	6174

Table 2. Number of hadrons and muons in $\overline{MU}$ data. $N_{h1}(N_{h2})$ and $N_{\mu 1}(N_{\mu 2})$ are the number of hadron events and muon events under (over) the R^B_{max} cut, respectively. A column MU is the number of events with the muon tag set.

References

1. E.Eichten, I.Hinchliffe, K.Lane and C.Quigg, Rev. Mod. Phys. 56, (1984) 579.

2. S.Aronson et al, Design Report for the DO Experiment at Fermilab Antiproton Proton Collider, Nov. 1984.

3. S.Iwata, Calorimetry, Nagoya University report DPNU-3-79 (1979).

4. R.K.Bock, T.Hansl-Kozanecka and T.P.Shah, Nucl. Instr. and Meth., 186 (1981) 533.

5. T. Hansel, WA1 collaboration, private communication.

6. I.A.Pless, E636 private communication, to be published.

7. J.Bofill et al., IEEE Trans. on Nucl. Sci. NS-29, (1982) 400.

8. (a) B.Rossi and K.Greisen, Rev. Mod. Phys. 13 (1941) 240.
(b) Particle Data Group, P.L., 111B (1982).

9. A.Bodek, CCFR data, private communication.

10. A. Bodek, University of Rochester report, UR911 (1985).

Figure Captions

Fig. 1. Schematic layout of the NW test beam apparatus.

Fig. 2. Multiplicity distributions and mean multiplicities for muon events in the A and B stations at 25, 50, 100, and 150 GeV/c.

Fig. 3. Fraction of muon events with multiplicity greater than one as a function of momentum.

Fig. 4. X-distributions in the A and B stations for muon events at 25, 50, 100, and 150 GeV/c. The solid histograms are for all muon events, while the dashed ones are for muon events with multiplicity=1.

Fig. 5. X-distribution in the A and B stations for muon events at 150 GeV/c with multiplicity>1.

Fig. 6. Exit angle and projected position standard deviation as a function of momentum for muon events. The solid (dashed) lines are calculated for station A(B).

Fig. 7. Muon momentum resolution as a function of momentum. Δ is the standard deviation in a Gaussian fit. The solid (open) points are uncorrected (corrected) for muons from pion decay.

Fig. 8. Multiplicity distributions and mean multiplicities for hadron events in the A and B stations at 50, 100, and 150 GeV/c.

Fig. 9. Multiplicity distribution in the B station for various A station multiplicities at a) 100 GeV/c and b) 150 GeV/c.

Fig. 10. X-distribution in the A and B stations for hadron events at 150 GeV/c. The solid (dashed) histograms are for the Standard (Beam) trigger events. The shaded area is for events with multiplicity, n_A=1. The arrows indicate the edges of the PDT chambers.

Fig. 11. Fitted values of Γ in stations A and B for incident momenta of 100 and 150 GeV/c.

Fig. 12. Hadron punchthrough probability as a function of momentum at various depths of absorber. Data points and heavy lines are the results of this experiment at two different depths. The rejection power of the Coulomb cut (Sec. 4.4) is also shown. For comparison, thin lines show data from iron absorber in other experiments. Two depths are shown for both WA1[5] and E636[6]. The deepest data are from CCFR[9].

Fig. 13. Maximum radial deviation in station B for muon events at 50, 100, and 150 GeV/c.

Fig. 14. Maximum radial deviation in station B for $\overline{MU}$ events at 50, 100, and 150 GeV/c.

Fig. 15. Maximum radial deviation in station B for hadron events at 50, 100, and 150 GeV/c.

Fig. 16. Schematic graph indicating the method used to separate $\overline{MU}$ events into hadronic and muonic contributions.

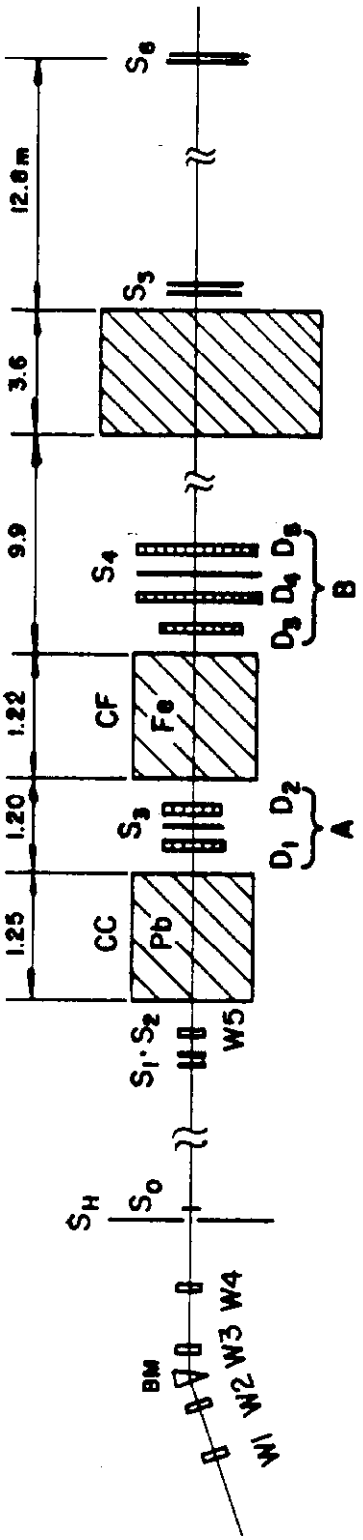
S6
12.6m
S3
3.6
9.9
S4
D3 D4 D5
B
1.22
CF
Fe
1.20
S3
D1 D2
A
1.25
CC
Pb
S1·S2
W5
SH
S0
BM
W1 W2 W3 W4

Fig. 1

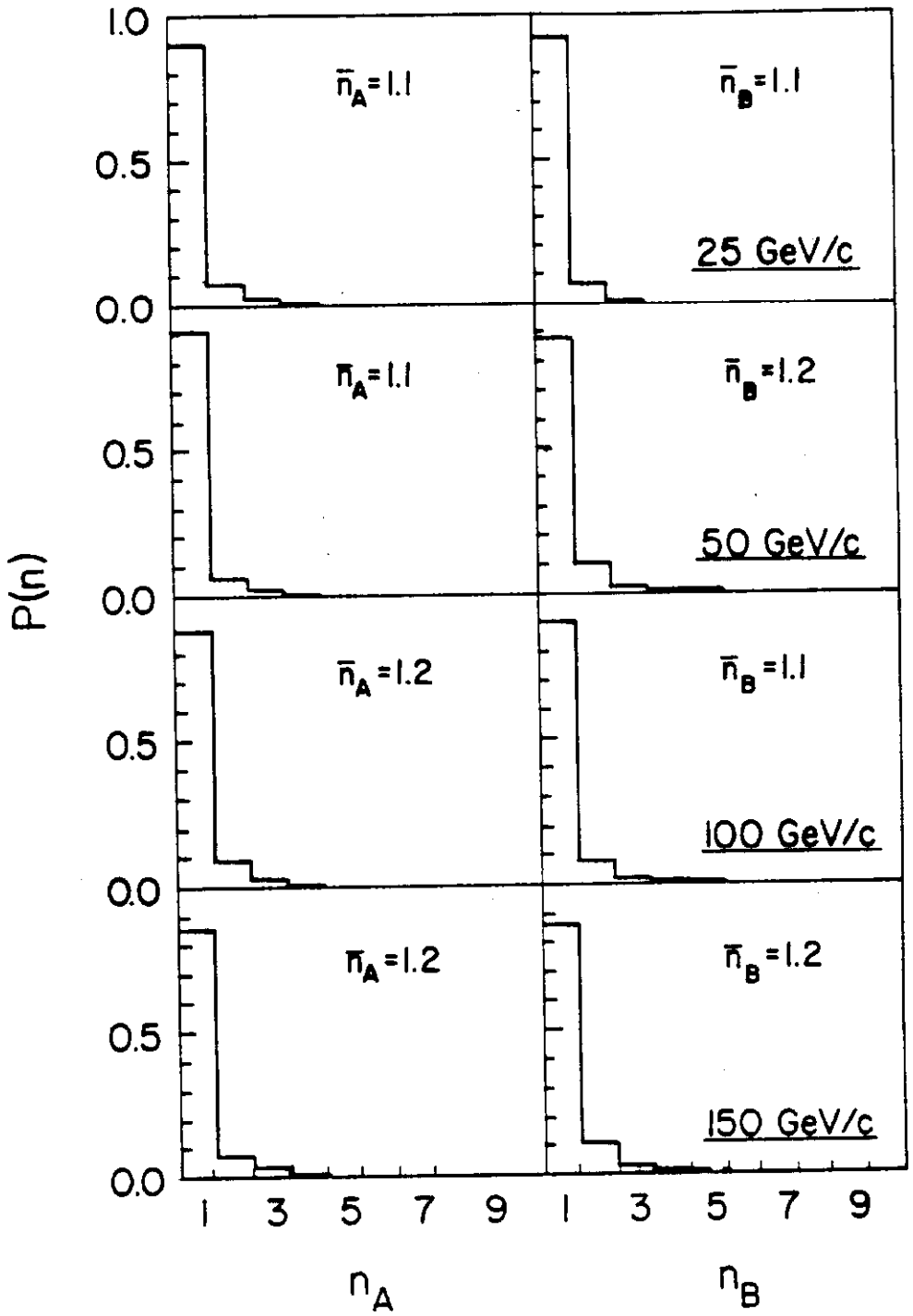
1.0
0.5
0.0
$\bar{n}_A$=1.1
$\bar{n}_B$=1.1
25 GeV/c
$\bar{n}_A$=1.1
$\bar{n}_B$=1.2
50 GeV/c
$\bar{n}_A$=1.2
$\bar{n}_B$=1.1
100 GeV/c
$\bar{n}_A$=1.2
$\bar{n}_B$=1.2
150 GeV/c
P(n)
1 3 5 7 9
n_A
n_B

Fig. 2

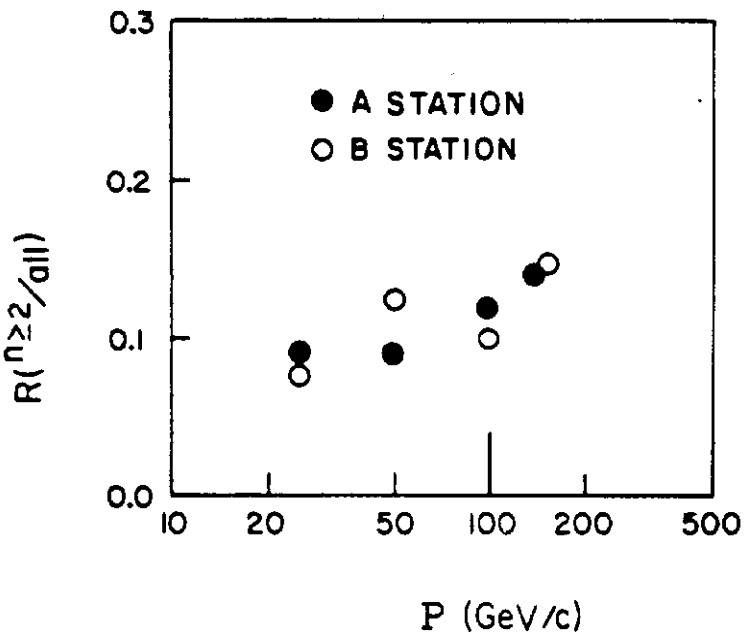
0.3
0.2
0.1
0.0
● A STATION
○ B STATION
R(n≥2/all)
10
20
50
100
200
500
P (GeV/c)

Fig. 3

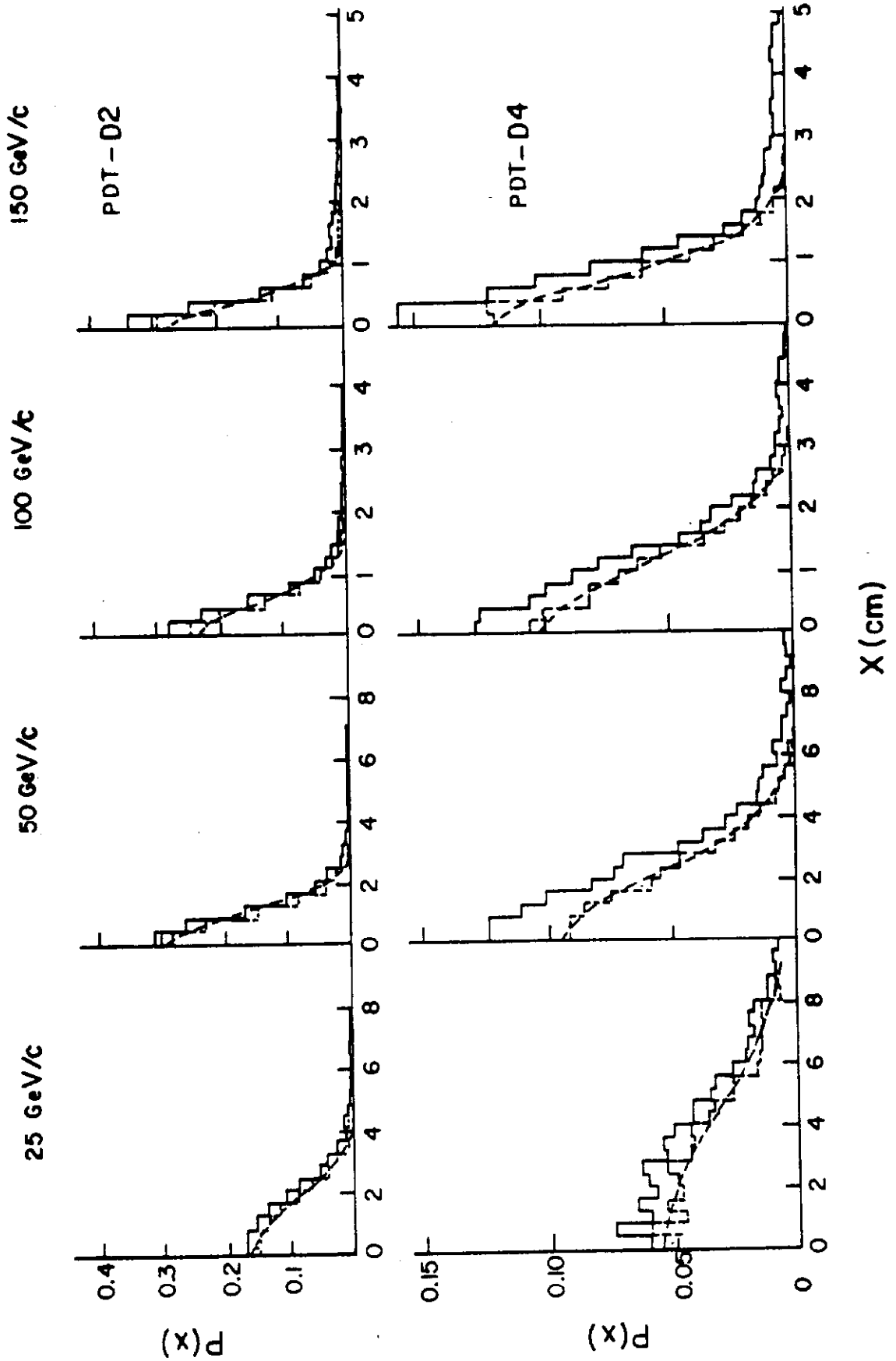

Fig. 4

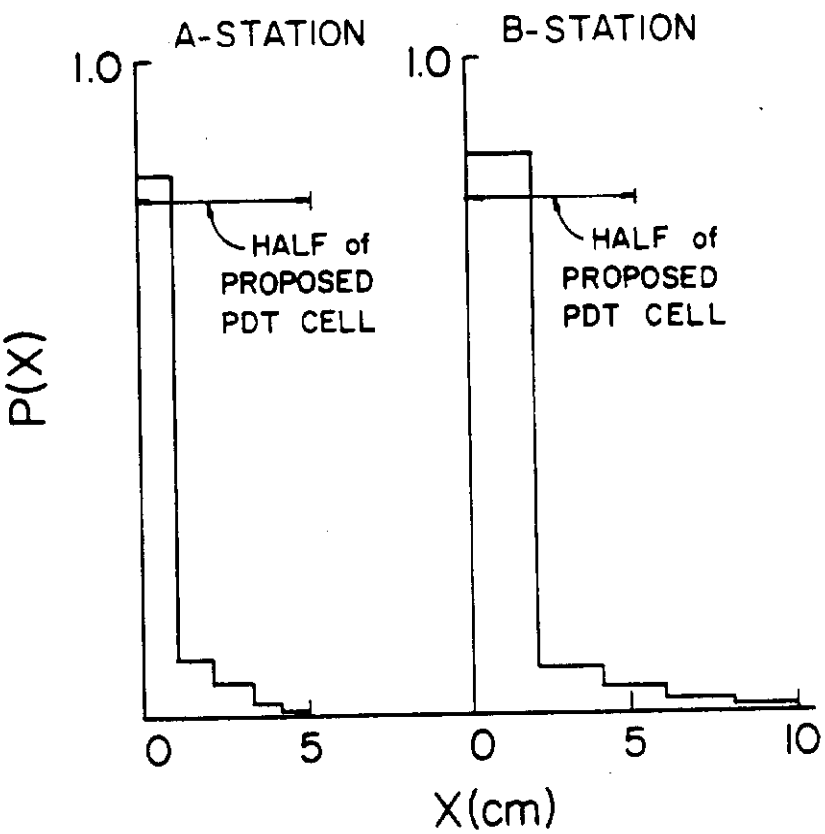
A-STATION
B-STATION
1.0
1.0
HALF of
PROPOSED
PDT CELL
HALF of
PROPOSED
PDT CELL
P(X)
0
5
0
5
10
X(cm)

Fig. 5

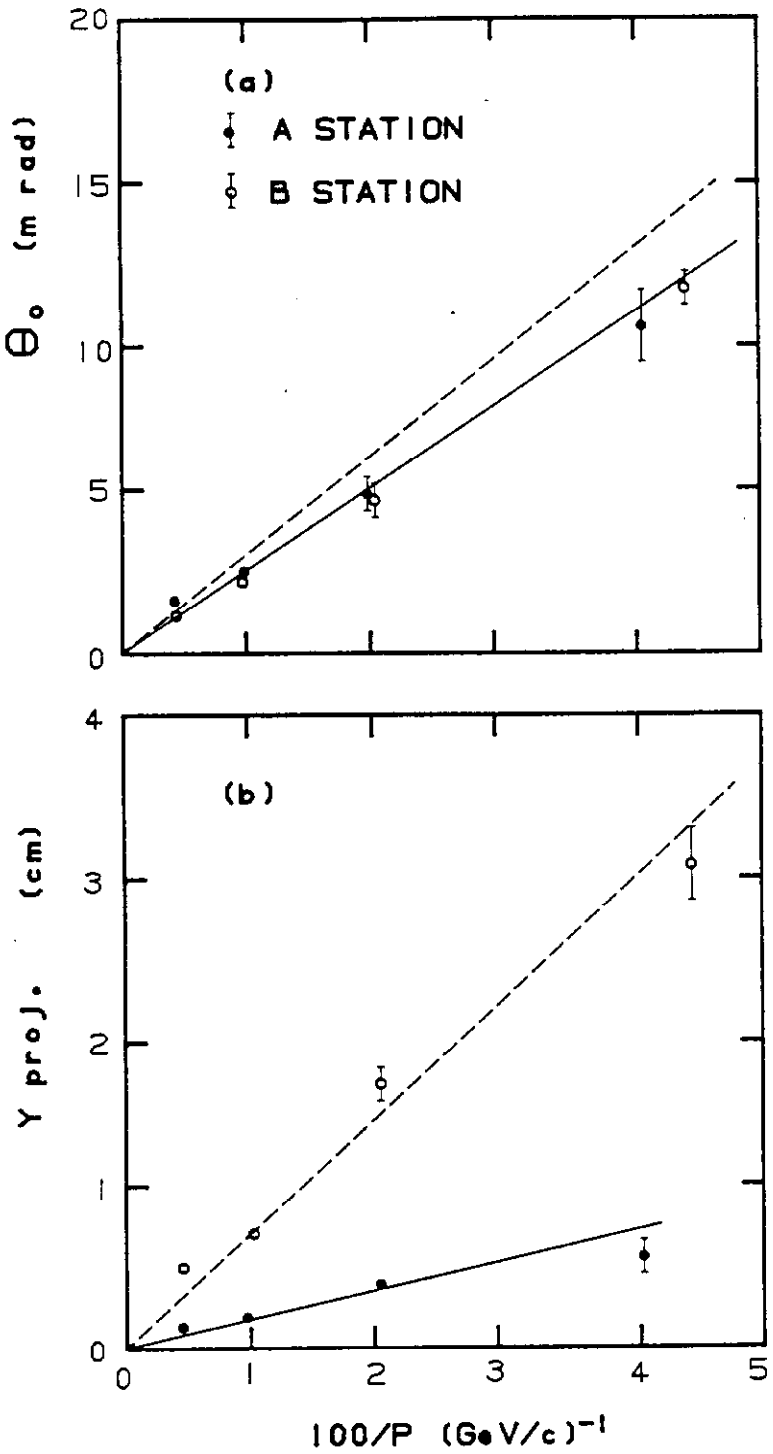
(a)
A STATION
B STATION
Θ_o (m rad)
20
15
10
5
0
(b)
Y proj. (cm)
4
3
2
1
0
0
1
2
3
4
5
100/P (GeV/c)$^{-1}$

Fig. 6

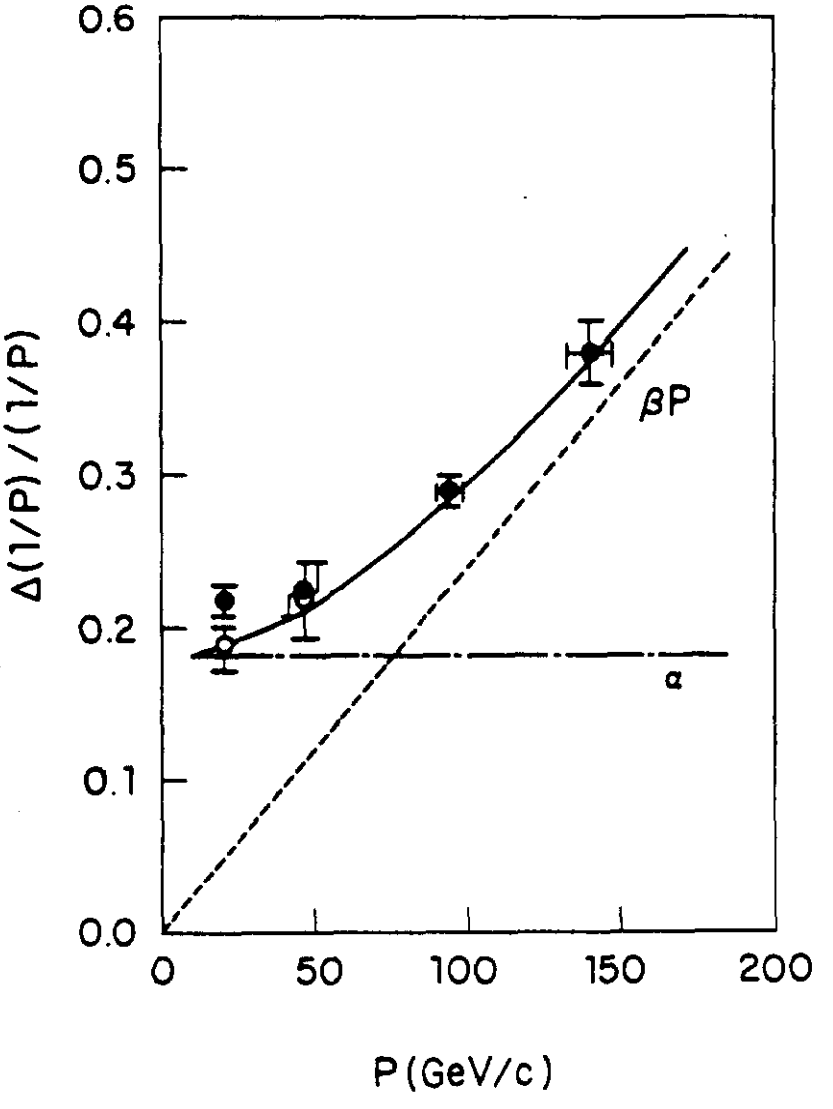

Fig. 7

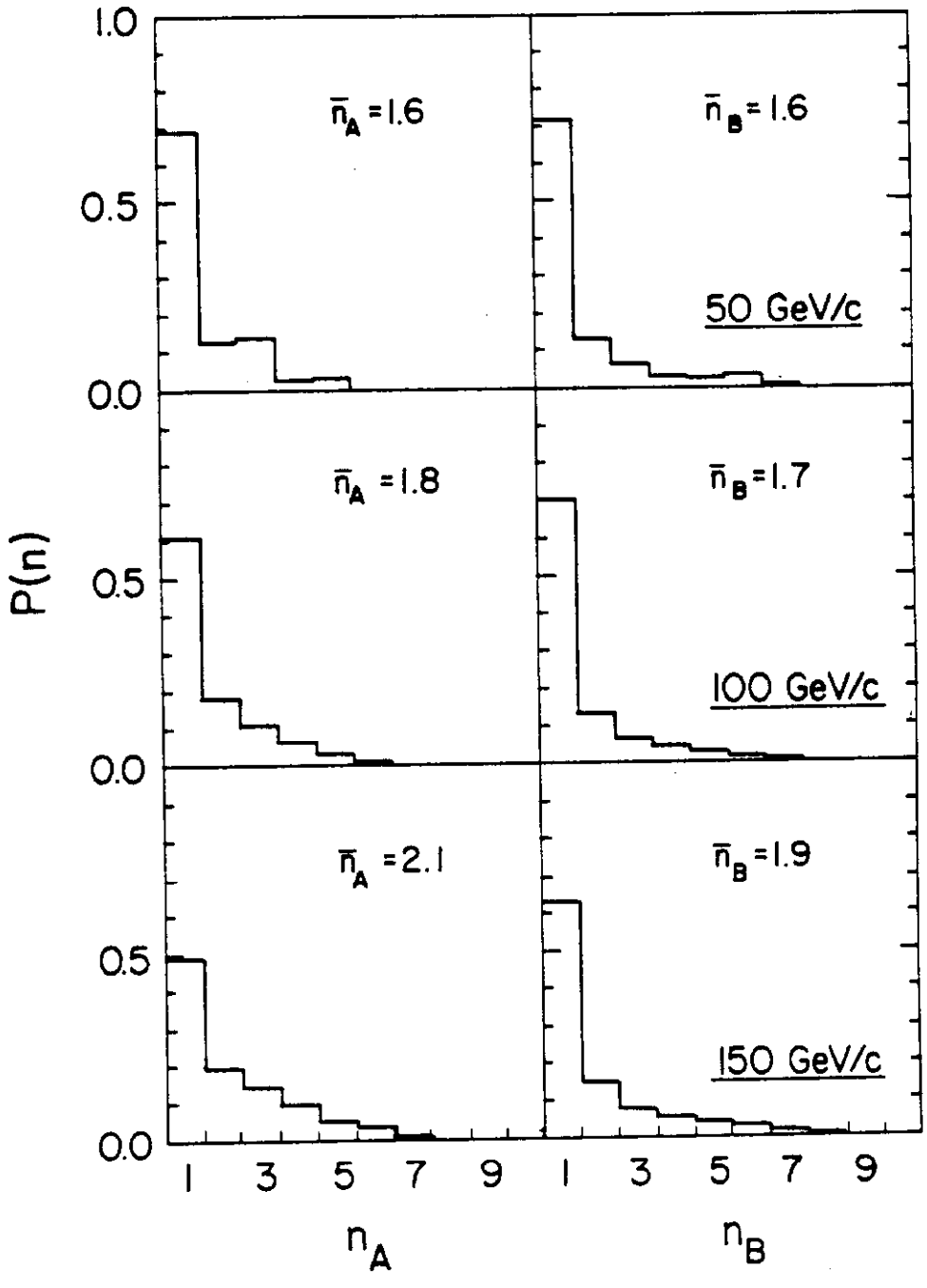
1.0
0.5
0.0
P(n)
$\bar{n}_A$ = 1.6
$\bar{n}_B$ = 1.6
50 GeV/c
$\bar{n}_A$ = 1.8
$\bar{n}_B$ = 1.7
100 GeV/c
$\bar{n}_A$ = 2.1
$\bar{n}_B$ = 1.9
150 GeV/c
1 3 5 7 9
n_A
1 3 5 7 9
n_B

Fig. 8

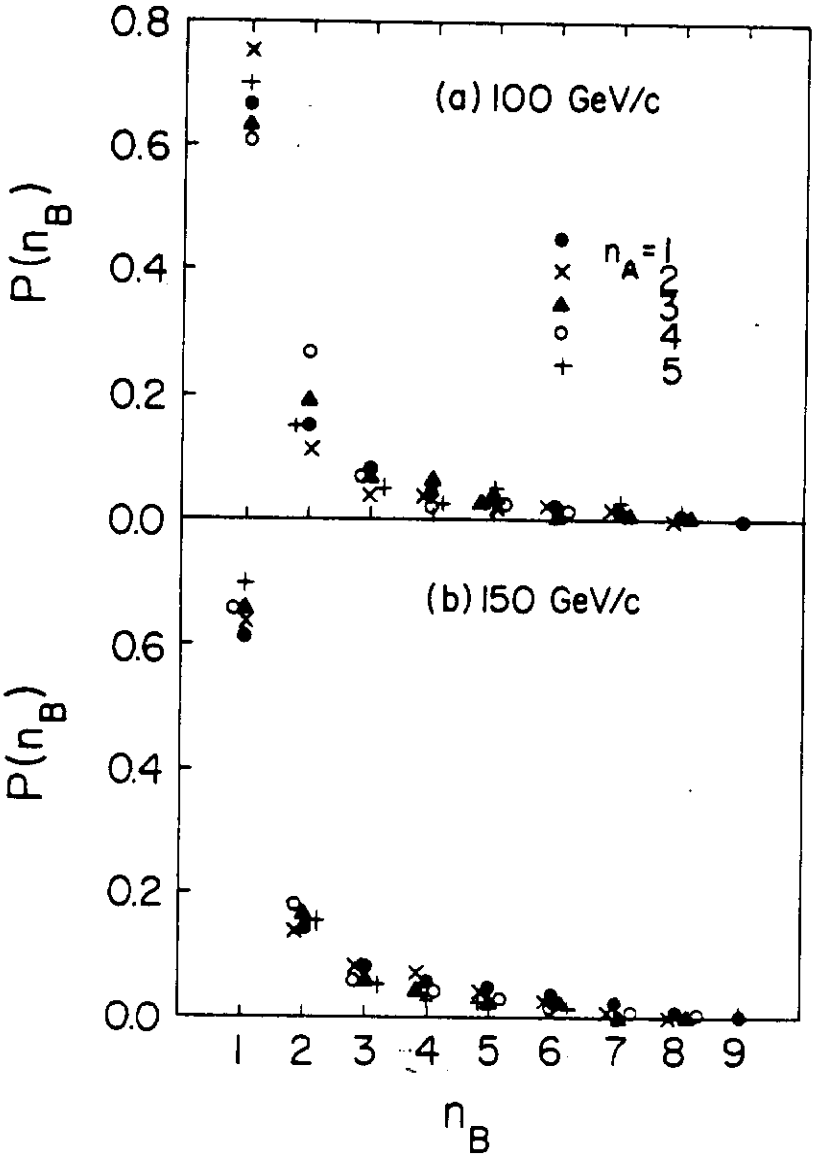

Fig. 9

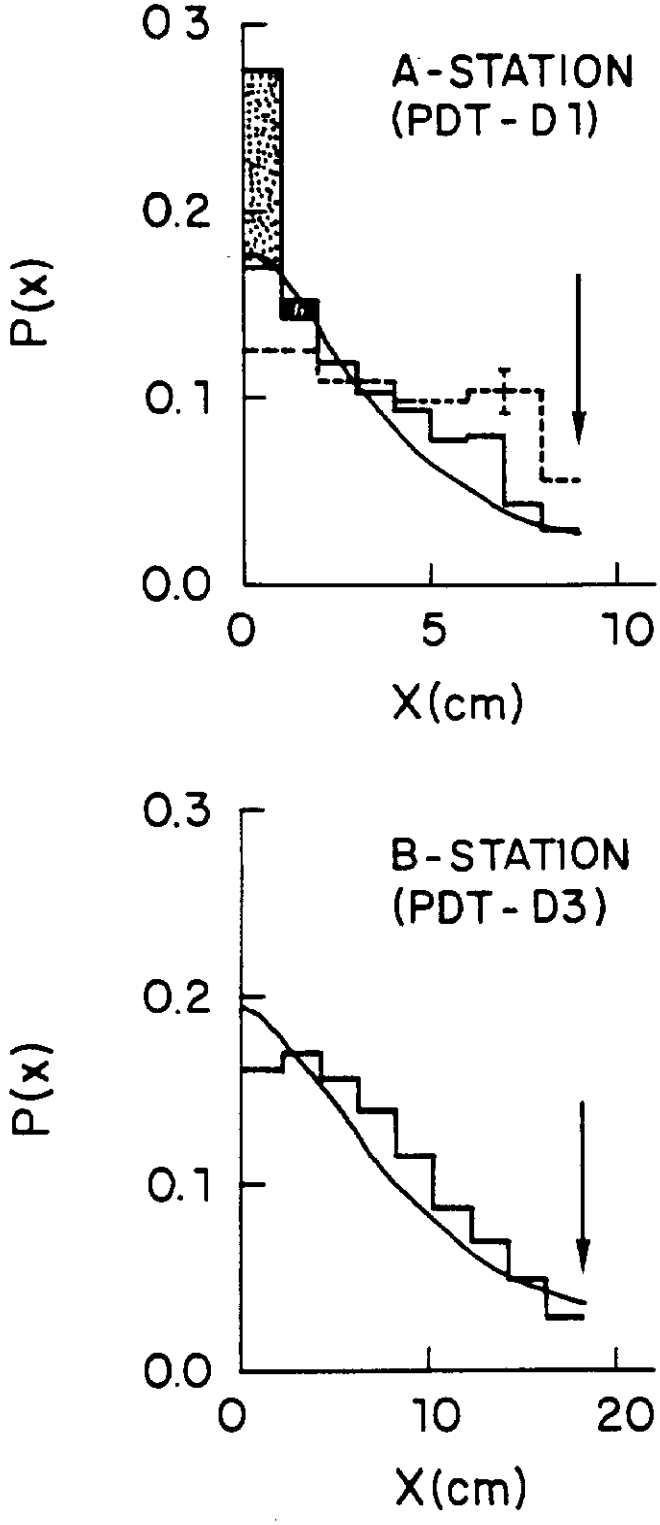
0.3
0.2
0.1
0.0
P(x)
A-STATION
(PDT-D1)
0
5
10
X(cm)
0.3
0.2
0.1
0.0
P(x)
B-STATION
(PDT-D3)
0
10
20
X(cm)

Fig. 10

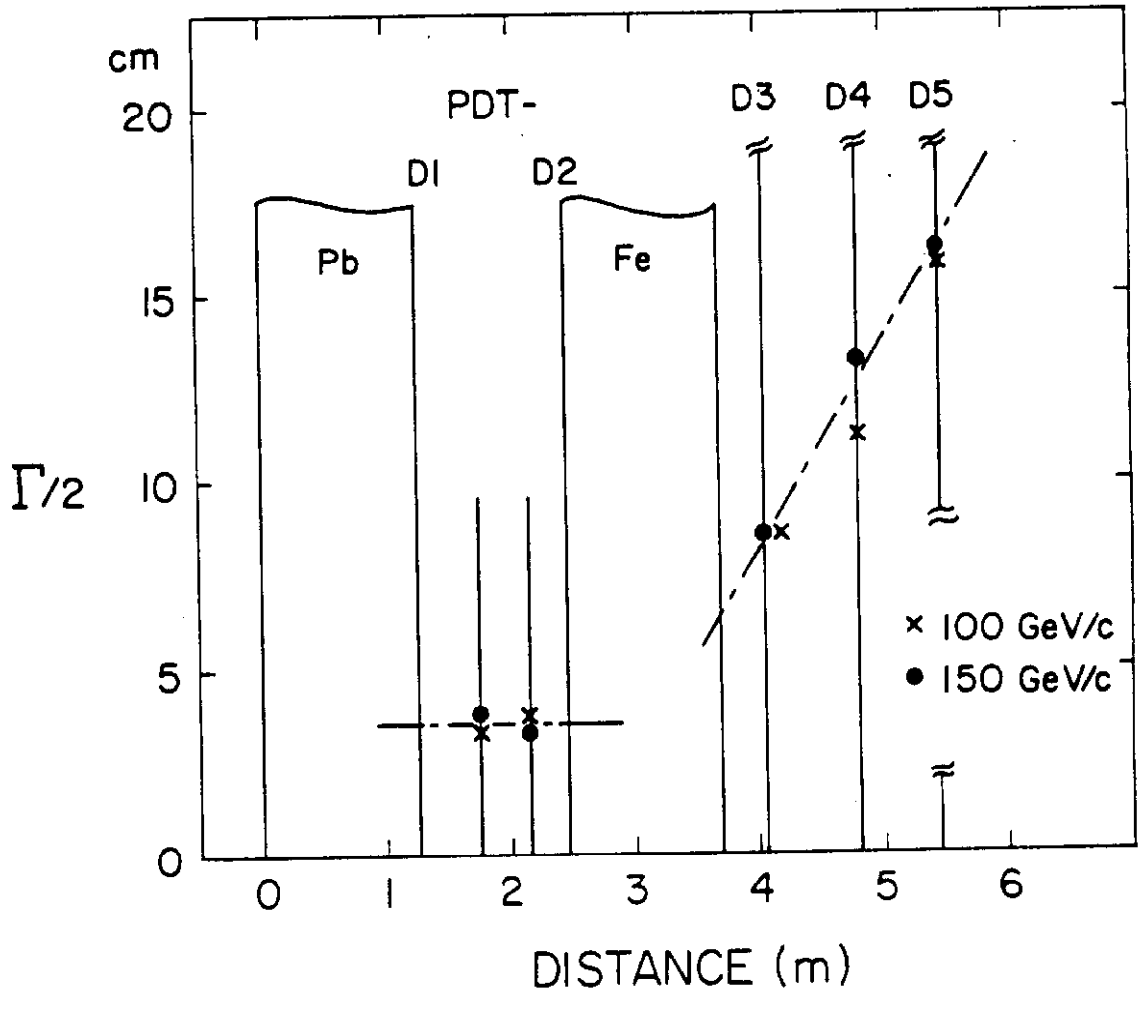
cm
20
15
10
5
0
Γ/2
PDT-
D1
D2
D3
D4
D5
Pb
Fe
× 100 GeV/c
● 150 GeV/c
0
1
2
3
4
5
6
DISTANCE (m)

Fig. 11

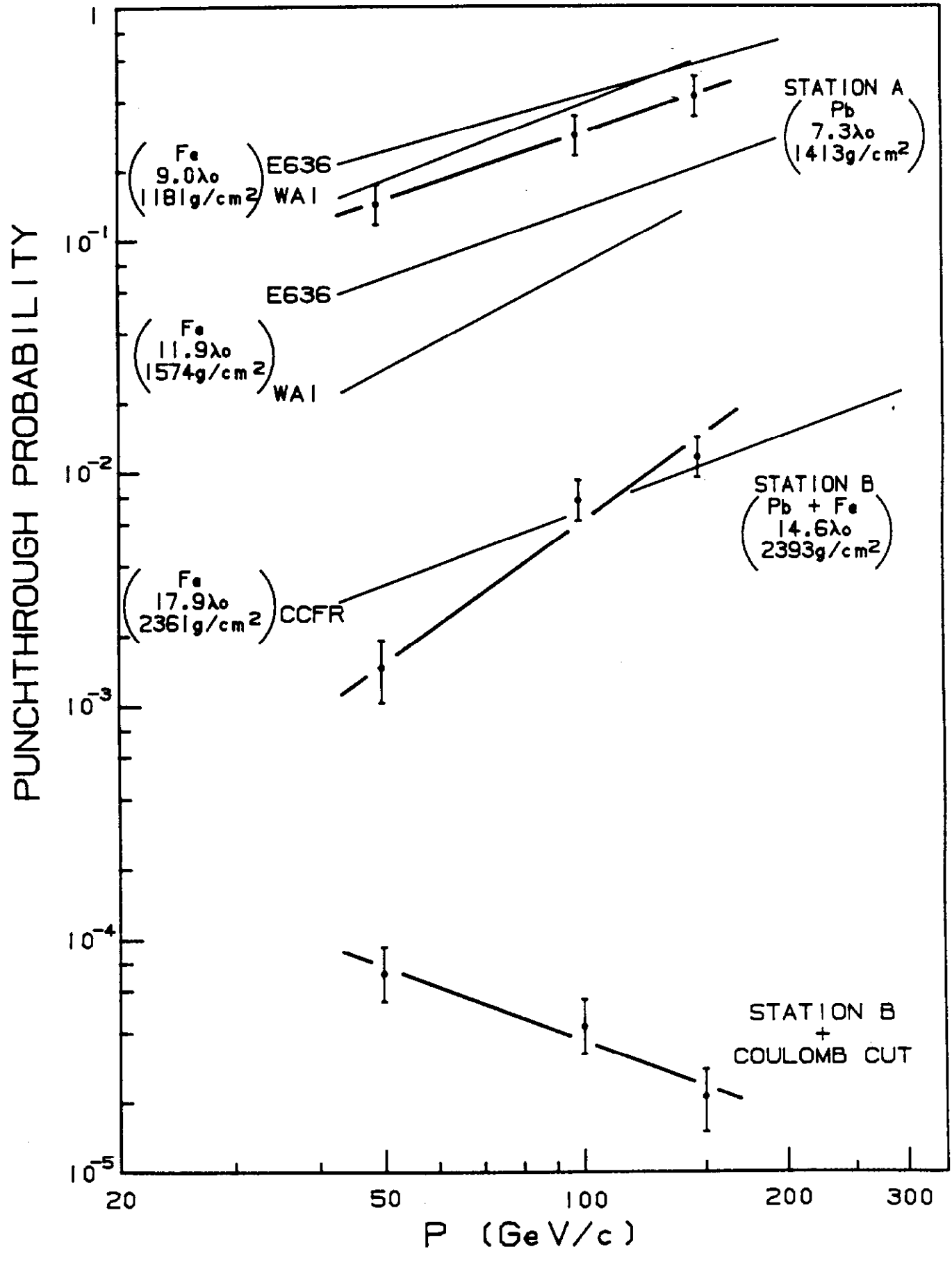
PUNCHTHROUGH PROBABILITY
1
10^{-1}
10^{-2}
10^{-3}
10^{-4}
10^{-5}
20
50
100
200
300
P (GeV/c)
STATION A
Pb
7.3λo
1413g/cm²
E636
WA1
Fe
9.0λo
1181g/cm²
E636
Fe
11.9λo
1574g/cm²
WA1
STATION B
Pb + Fe
14.6λo
2393g/cm²
Fe
17.9λo
2361g/cm²
CCFR
STATION B
+
COULOMB CUT

Fig. 12

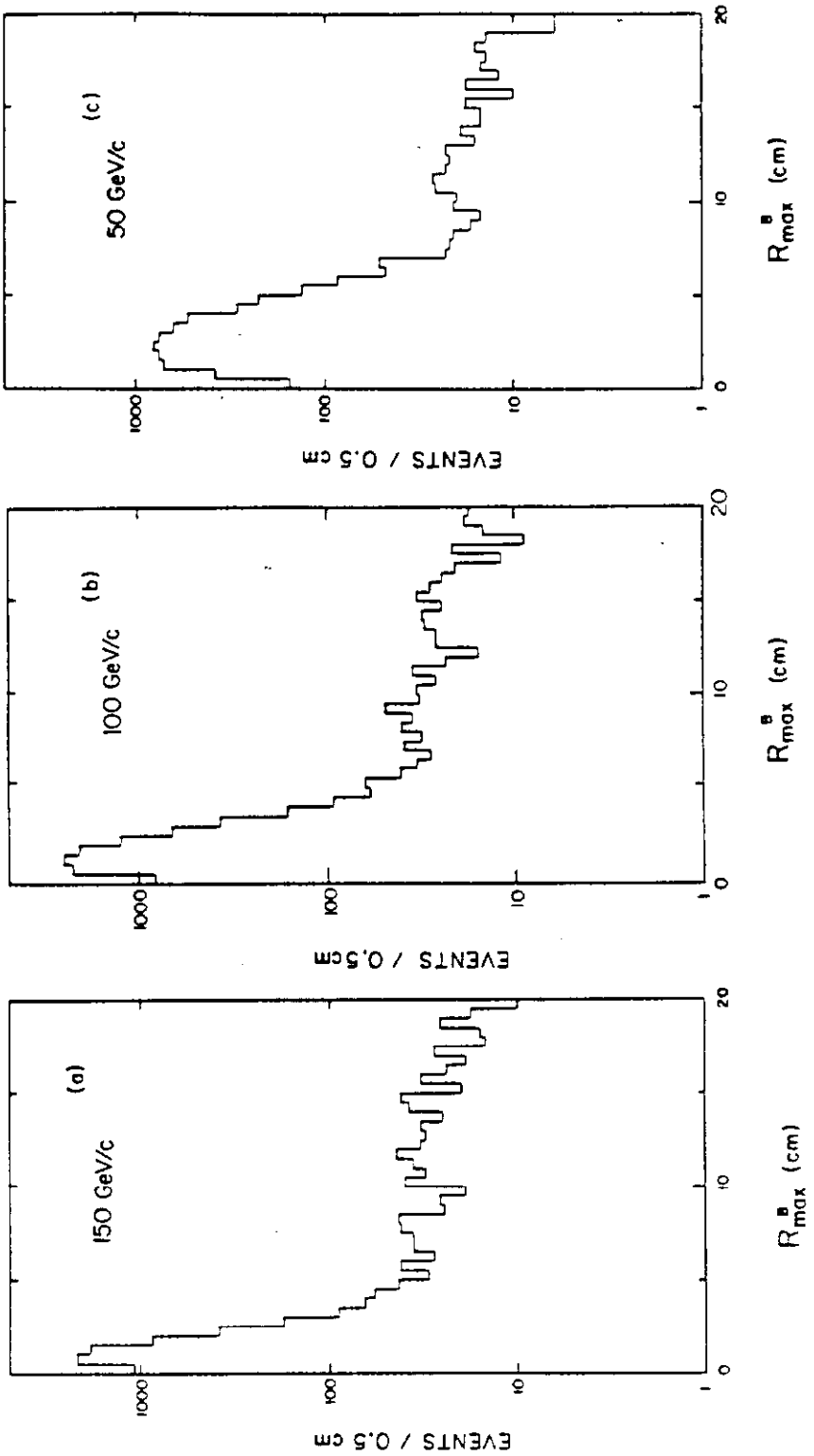

Fig. 13

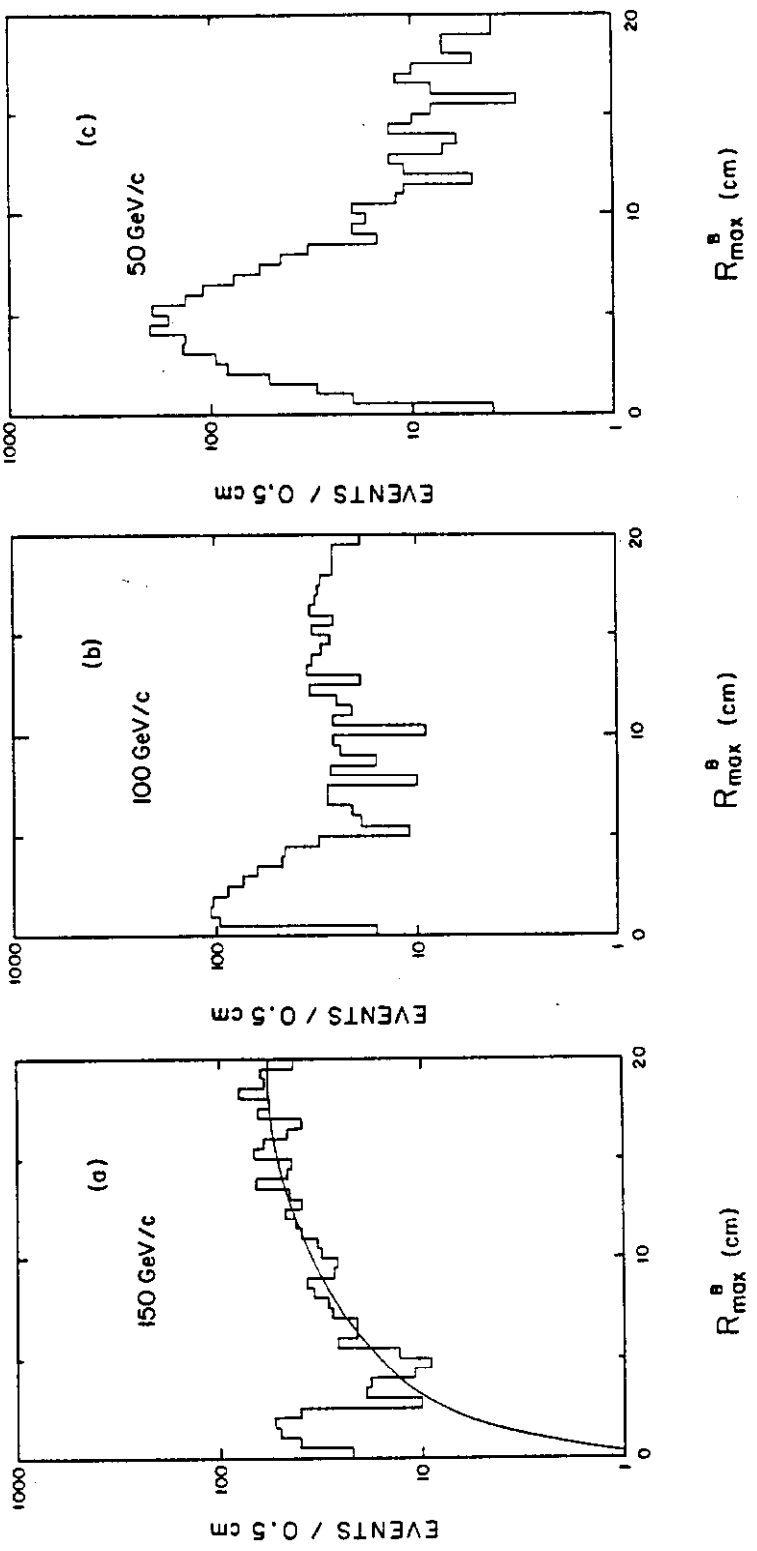
(a)
150 GeV/c
(b)
100 GeV/c
(c)
50 GeV/c
EVENTS / 0.5 cm
1000
100
10
1
0
10
20
R^B_{max} (cm)

Fig. 14

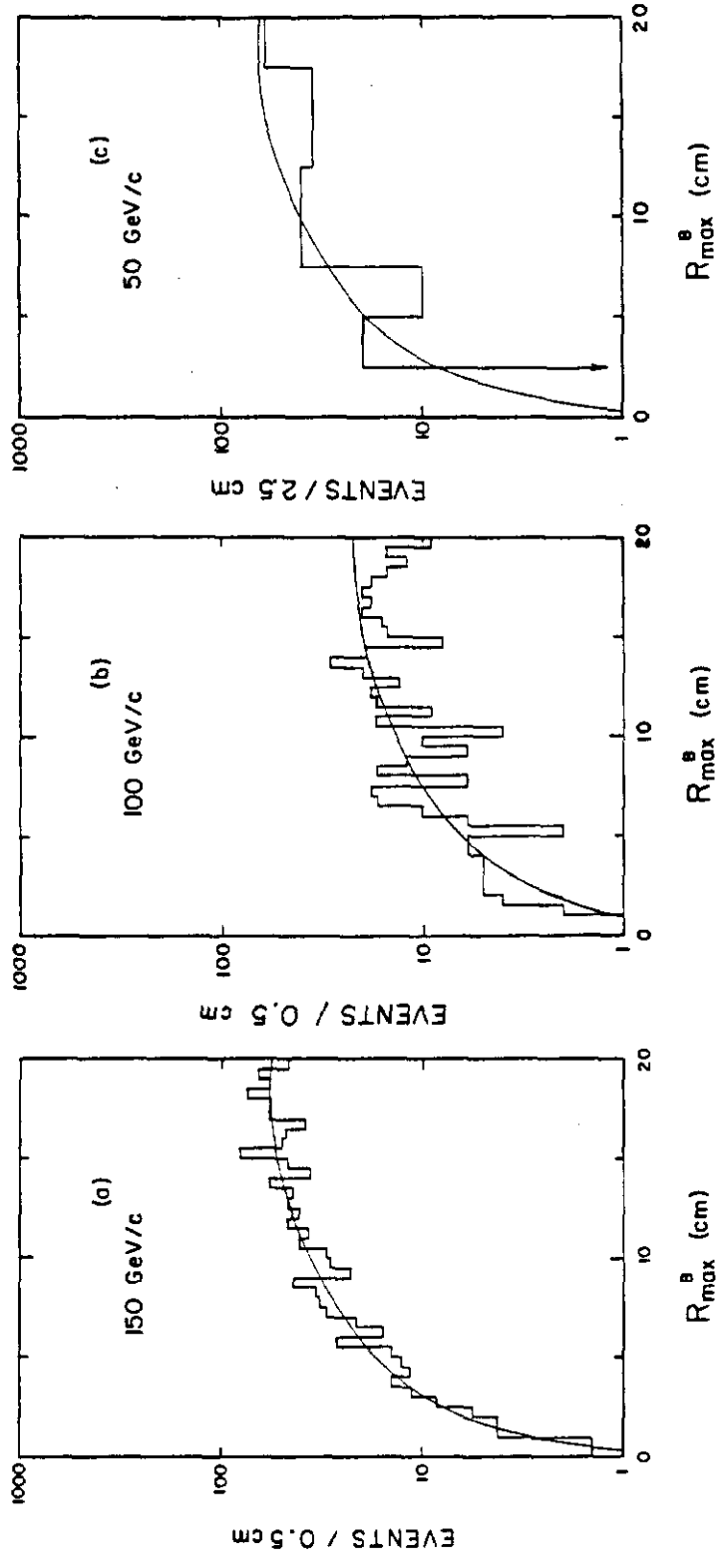
(a)
150 GeV/c
EVENTS / 0.5 cm
(b)
100 GeV/c
EVENTS / 0.5 cm
(c)
50 GeV/c
EVENTS / 2.5 cm
R^B_{max} (cm)
1000
100
10
1
0
10
20

Fig. 15

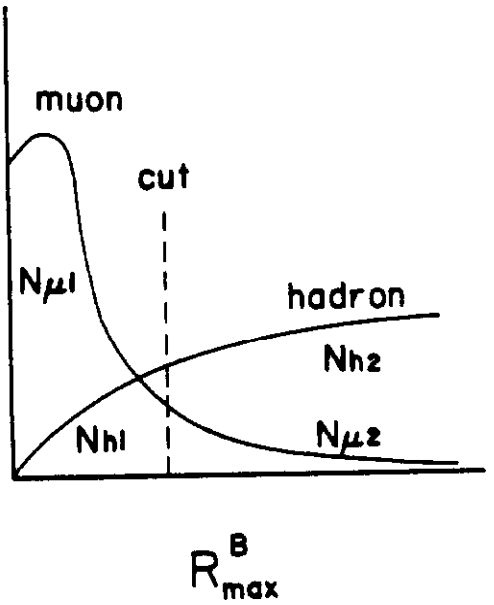

Fig. 16